Entrance channel effects in the fusion-fission time scales from studies of prescission neutron multiplicities

A. Saxena, A. Chatterjee, R. K. Choudhury, S. S. Kapoor, and D. M. Nadkarni
Nuclear Physics Division, Bhabha Atomic Research Centre, Bombay 400085, India
(Received 16 June 1993)

Prescission neutron multiplicities in fusion-fission reactions of ^{11}B+^{237}Np, ^{11}B+^{232}Th, ^{12}C+^{232}Th, and ^{16}O+^{232}Th, lying on either side of the Businaro-Gallone mass asymmetry (α_{BG}), have been measured. The present data along with those available in literature for compound systems spanning the fissility range from 0.70 to 0.84 were analyzed in a consistent manner to deduce fusion-fission time scales for all systems. From the systematic behavior of all the data, the three components of total dynamical fusion-fission delay, namely, transient delay, saddle-to-scission delay, and formation delay, have been deduced. It is found that the formation delay depends on the entrance channel mass asymmetry relative to Businaro-Gallone point. The variations of the fusion-fission time scales with fissility, ratio of fission barrier to temperature, and entrance channel mass asymmetry have been studied.

PACS number(s): 25.70.Jj

I. INTRODUCTION

In recent years there have been numerous measurements [1–10] of fragment neutron angular correlations in heavy-ion-induced fusion-fission reactions to determine the average prescission neutron multiplicities M_n^{pre} over a large range of bombarding energies and compound nuclear masses. It is now well established that the measured prescission neutron multiplicities are, in general, much larger than those expected on the basis of neutron, charged particle, and fission widths calculated from statistical models with the level density parameters adjusted to explain the observed fission excitation functions. The excess neutron emission from the composite fissioning nucleus has been interpreted to be due to a time delay in the fission process arising due to dynamical effects in the fission decay. Thus these studies have provided a valuable "clock" in the time scale of 10^{-20}–10^{-21} s to probe the dynamics of the fusion-fission process. It was shown by Weidenmuller and co-workers [11–13] and Grange [14] based on the pioneering work of Kramers [15] that diffusion from the equilibrium configuration to the saddle point takes over a finite transition time due to nuclear viscosity effects and therefore the fission width rises to its final quasistationary value over a finite time. This is one of the processes which results in a time delay in the fission process (termed the transient delay τ_{tr}). Neutron emission during this time delay can be an important source of excess prescission neutrons.

A second contribution to the number of excess prescission neutrons is also expected due to neutron emission from the dynamical evolution during the saddle-to-scission transition time τ_{SS}. The dependence of τ_{SS} on the fissility of the compound nucleus has been theoretically investigated by many authors [16,17]. The third source of prescission neutrons can be due to nuclear deexcitation by neutron emission of the temperature-equilibrated intermediate dinuclear complex during the time τ_{fo} of its evolution toward compound nucleus formation. In heavy-ion fusion reactions, the energy equilibration takes place [18] in a time scale of 10^{-22} s, while the evolution toward a fully equilibrated compound nucleus takes [19] much longer ($\approx 10^{-20}$ s). Hence the dinuclear complex can be considered to be temperature equilibrated at different points and can emit neutrons during evolution toward the compound nucleus. One way to look for contributions to neutron emission during the compound nucleus formation phase is to carry out measurements on different projectile-target systems leading to the same compound nucleus but having different formation times expected due to the difference in the fusion dynamics. It is known [20–23] that the entrance channel mass asymmetry $\alpha = (A_t - A_p)/(A_t + A_p)$ plays an important role in the dynamical evolution of the temperature-equilibrated dinuclear system leading to compound nucleus formation and the fusion path followed by the composite system is quite different for the two cases of $\alpha < \alpha_{BG}$ and $\alpha > \alpha_{BG}$, where α_{BG} is the critical Businaro-Gallone mass asymmetry. In the present work, we have carried out measurements of prescission neutron multiplicities for the fissioning systems of ^{11}B+^{232}Th, ^{12}C+^{232}Th, ^{11}B+^{237}Np, and ^{16}O+^{232}Th fissioning systems, of which the first three systems correspond to $\alpha > \alpha_{BG}$ and the last system corresponds to $\alpha < \alpha_{BG}$ (see Table I). Also, the ^{11}B+^{237}Np and ^{16}O+^{232}Th systems populate the same compound nucleus ^{248}Cf, and, therefore, any difference in the prescission neutron multiplicities in these reactions would directly reflect on the compound nucleus formation time τ_{fo} in these systems. The present data along with those available in the literature for compound systems in the fissility range of $0.7 < x < 0.84$ were analyzed in a uniform way to extract fusion-fission delays in all the systems. The dependence of the fusion-fission delay on the various parameters such as B_f/T, x, and α has been examined in detail. The data were parametrized within the framework of the transient delay theory [11–14] to deduce τ_{tr}, τ_{SS}, and τ_{fo} in a self-consistent way. It is seen that, among other pa-

 ©1994 The American Physical Society

rameters, entrance channel mass asymmetry plays a role in the determination of the fusion-fission delay. In the following sections, the experimental setup, data analysis procedure, and results are discussed.

II. EXPERIMENTAL PROCEDURE

The experiments were performed using ^{11}B, ^{12}C, and ^{16}O beams obtained from the Bhabha Atomic Research Centre-Tata Institute of Fundamental Research 14UD Pelletron accelerator. Figure 1 shows a schematic diagram of the experimental setup used. A self-supporting ^{232}Th target of 1.8 mg/cm^2 thickness and a 300 μg/cm^2 ^{237}Np target on aluminum backing were used in the experiment with the target plane making an angle of 70° with respect to the beam direction. Two thin silicon surface barrier detectors ($\approx$ 12 μm) were placed at angles of 110° and 160° with respect to the beam direction to detect the fission fragments. A thin-walled scattering chamber was used to minimize multiple neutron scattering. Two NE213 neutron detectors (5 cm thick and 5 cm in diameter) were positioned outside the scattering chamber at a distance of 50 cm from the target such that each of these detectors subtended angles of 0° (or 180°) and 90° with respect to the direction of fragment detection. In this way, fragment-neutron angular correlations for four combinations of fragment and neutron detection angles could be measured without moving the neutron detectors. This is important since the measured efficiency of a neutron detector can vary with position due to surrounding materials. The time-of-flight signal of each neutron detector was obtained with reference to the start pulse derived from either of the two fission detectors. The time jitter in the time-of-flight signal as a function of fragment pulse height was corrected to minimize the spread. The time resolution was found to be 2.5 ns as seen from the full width at half maximum of the prompt gamma-ray peak in the time-of-flight spectrum. The position of the gamma-ray peak in the time-of-flight spectrum was used as the reference for calibrating the time-of-flight signal. In order to keep the background in the time-of-flight spectra at a minimum level, the beam dump was kept at a distance of about 2 m from the target and was well shielded with layers of lead and borated paraffin. A further reduction in the gamma background

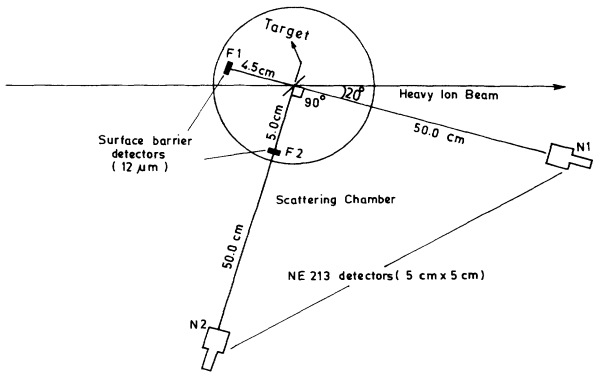

FIG. 1. Schematic representation of the experimental setup.

is achieved after employing the pulse shape discrimination technique to differentiate neutrons and gamma rays in the neutron detectors. This was done by appropriate gating in the two-dimensional plot of pulse shape versus pulse height of the neutron detectors. The parameters consisting of time of flight, pulse shape signal, dynode signal of the two neutron detectors, and the fission fragment pulse height from the two fragment detectors were recorded such that the events corresponding to each of the four combinations of fission-neutron coincidences could be distinguished. Fission events without coincidence with neutrons were also recorded after suitably scaling them down for the purpose of obtaining the neutron yield per fission in the experiment.

The detection efficiency of each of the neutron detectors was experimentally determined in a separate experiment by measuring neutron time-of-flight spectrum in coincidence with fission fragments from a ^{252}Cf source in 2π geometry and comparing the measured energy spectrum with the empirical form given by Madland and Nix [24].

III. DATA ANALYSIS AND RESULTS

The laboratory neutron energy spectra were determined from the observed time-of-flight spectra after correcting for the neutron detection efficiency for each neutron detector. Some typical spectra are shown in Figs. 2 and 3. In order to obtain the prescission and postscission neutron components, the observed neutron energy spectra were fitted with three moving-source evaporation components (the prescission component corresponding to emission from composite nucleus and the postscission components corresponding to emission from the two fission fragments) using the Watt expression [25]:

$$Y(E_n) = \sum_{i=1}^{3} \frac{M_n^i \sqrt{E_n}}{2(\pi T_i)^{3/2}} \times \exp\left(\frac{-(E_n - 2\sqrt{\epsilon_i E_n}\cos\phi_i + \epsilon_i)}{T_i}\right), \quad (1)$$

where ϵ_i, T_i, and M_n^i are the energy per nucleon, temperature, and multiplicity of each neutron emission source i. E_n is the laboratory energy of the neutron, and ϕ_i is the neutron detection angle with respect to the source i. The above expression is based on the reasonable assumption of isotropic neutron emission in the rest frame of the emitting systems. The ϵ_i value for the composite nucleus was calculated assuming full momentum transfer since the contribution due to transfer-induced fission is expected to be small at energies used in the experiment. The ϵ_i values for the two fission fragments and the angle of emission of the complementary fragment were determined by applying the reaction kinematics using the Viola's systematics for total kinetic energy release for the symmetric division [26]. The postscission parameters $M_n^{\rm post}$ and $T_{\rm post}$ for both fragments were assumed to be equal. The temperature for the prescission component $T_{\rm pre}$ was also fixed using a Fermi gas relation between temperature and excitation energy assuming the

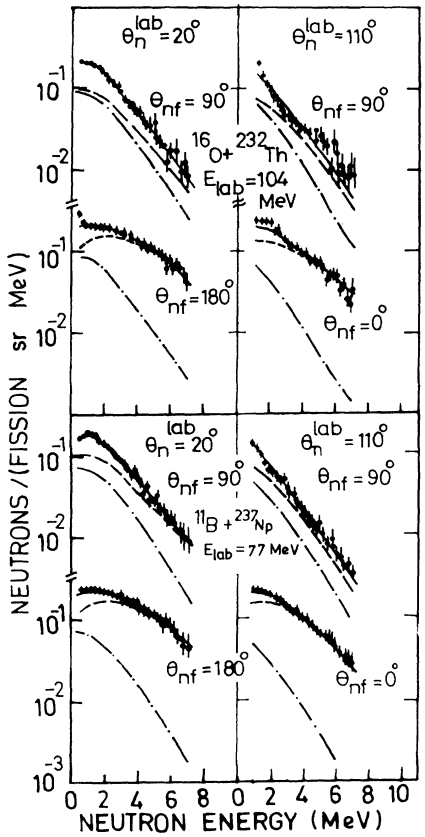

FIG. 2. Measured neutron energy spectra for the two neutron detectors at angles of 0° (or 180°) and 90° with respect to the fission direction along with the fits for $^{16}O+^{232}Th$ and $^{11}B+^{237}Np$ systems. The dashed, dash-dotted, and solid lines show the contributions of the postscission component, prescission component, and the sum of the two, respectively.

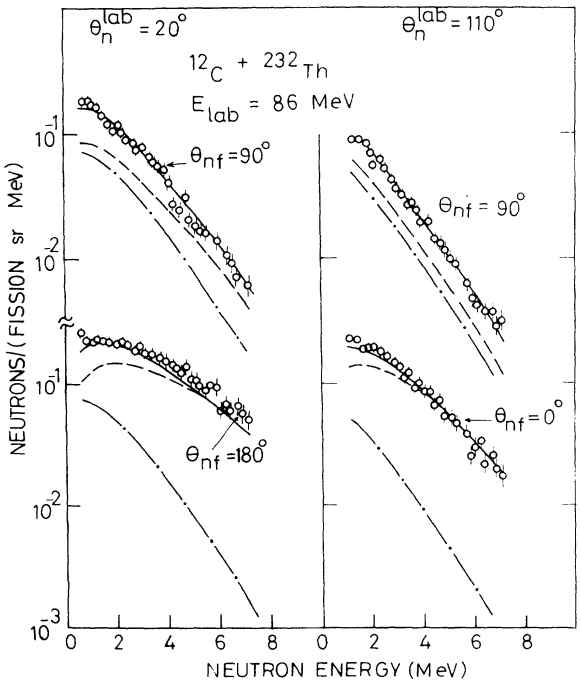

FIG. 3. Same as Fig. 2 but for the $^{12}C+^{232}Th$ system.

level density parameter to be given by $a_n = A_{CN}/10.0$ MeV^{-1}:

$$a_n T^2(E_x) = E_x - S_n - 2T(E_x), \tag{2}$$

where A_{CN} and E_x are mass and initial excitation energy of the compound nucleus, T is the temperature of the first residual nucleus, and S_n is the separation energy of the neutron. According to LeCouteur and Lang [27,28], a factor of $\frac{11}{12}$ takes care of the cascade of sequential particle evaporation and T_{pre} is taken as $\frac{11}{12}T(E_x)$. The remaining parameters T_{post}, M_n^{post}, and M_n^{pre} were obtained by fitting the observed spectra with Eq. (1) by the χ^2 minimization procedure. Figures 2 and 3 also show the typical fits to the neutron energy spectra for different systems. The sensitivity of the fits to the various parameters was checked by calculating the change in χ^2 due to a small change in the values of the parameters. Minimum values of χ^2/(degrees of freedom) are in the range of 0.8–1.20 for different spectra. It was seen that a small change in M_n^{pre} or M_n^{post} by about 10% from the minimized values gives an increased χ^2/(degree of freedom) by about 12%–26%, resulting in noticeably poor fits to the observed spectra. Fits were also obtained using T_{pre} as a free parameter. However, the results on neutron multiplicities were found to be close within errors to those obtained by fixing T_{pre} as discussed above. In the present experiment, the values of M_n^{pre} and M_n^{post} were determined from two independent sets of data, one measured with the neutron detector at 20° and the other at 110°. The values of the M_n^{pre} and M_n^{post} obtained from these two sets were found to be consistent with each other, which implies that there is no appreciable dependence of M_n^{pre} and M_n^{post} on the neutron detection angle with respect to the beam direction. From the fitted values of M_n^{pre} and M_n^{post}, the total neutron multiplicity was derived as $M_n^{tot} = M_n^{pre} + 2M_n^{post}$. Figure 4 shows the correlation between the values of M_n^{pre} and M_n^{tot} for the systems measured in the present work along with the data for other systems taken from the literature. The present data agree with the overall trend indicated by the straight line with a slope of 0.62±0.09 and an offset for $M_n^{pre} = 0$ corresponding to $M_n^{tot} = 3.15 \pm 0.3$.

Figure 5 shows the variation of M_n^{tot} with excitation energy of the compound nucleus for different target-projectile systems measured in the present work. It is seen from this figure that as expected M_n^{tot} increases with excitation energy for all the systems. It is also seen that for the $^{12}C+^{232}Th$ projectile-target system, corresponding to the ^{244}Cm compound nucleus, the total neutron multiplicity at a given excitation energy is smaller than that for the ^{248}Cf compound system as expected due to lower fissility in the former case. Also, it is interesting to note that for the $^{11}B+^{237}Np$ and $^{16}O+^{232}Th$ systems, both populating the same compound nucleus ^{248}Cf, the observed values of M_n^{tot} at any given excitation energy appear to be nearly equal.

Figure 6 shows the variation of M_n^{pre} with excitation energy for the various systems. The dashed lines correspond to straight line fits through the data points for different systems. It is seen from this figure that

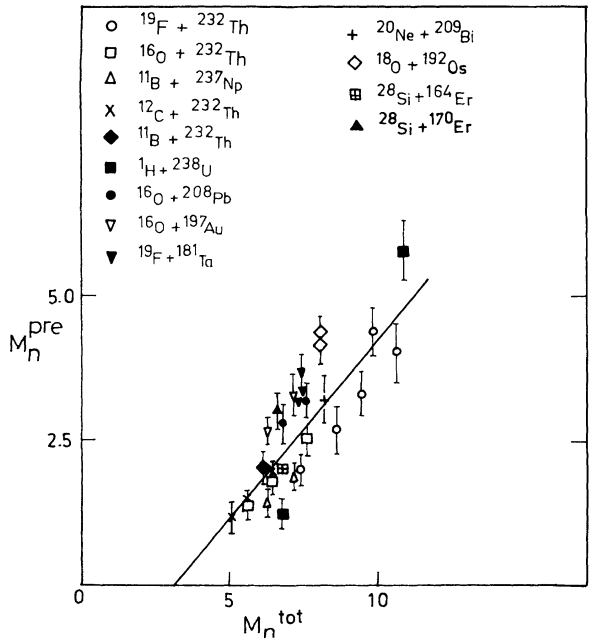

FIG. 4. Average prescission versus average total neutron multiplicity for the present measurements along with data from the literature. References for the data points are listed in Table I.

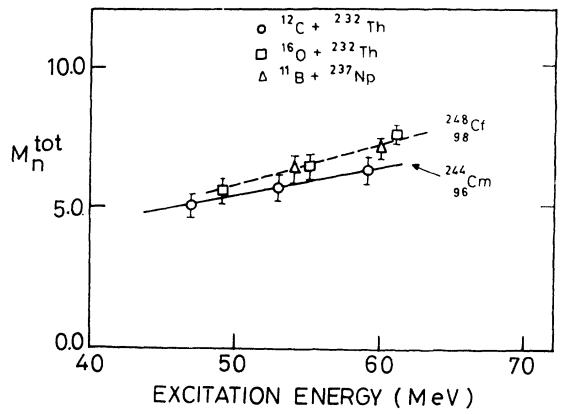

FIG. 5. Experimental average total neutron multiplicity as a function of the excitation energy of the compound nucleus for various target-projectile systems. The lines correspond to straight line fits to the data for the two compound systems.

the $^{16}O+^{232}Th$ system gives a larger prescission neutron multiplicity as compared to the $^{11}B+^{237}Np$ system at a given excitation energy. This result implies that entrance channel mass asymmetry plays a role in determining the fusion-fission time scales in these systems. In Fig. 6 we also show the values of prescission neutron multiplicities expected from the statistical model calculation using the PACE2 code [29] for values of the level density parameter a_n in the range of $A/7.5$–$A/10.0$ MeV^{-1} and $a_f/a_n = 1.0$ for different systems. The above choice of parameters seems reasonable since for the values of $a_n = A/10.0$ MeV^{-1} and $a_f/a_n = 1.0$ the measured fusion-fission excitation functions [20] are described rather well. It is apparent from this comparison that a considerable number of excess neutrons in the prescission phase are emitted in all cases. Furthermore, the number of excess neutrons increases with the excitation energy.

Neutron emission during fragment acceleration tends to lower the resulting values of M_n^{post} and give increased values for M_n^{pre}. Using the formalism of Eismont [30], it is seen that the fragment acceleration time is of the order of 5.5×10^{-21} s for ^{248}Cf and ^{244}Cm fissioning systems and the neutron evaporation time, calculated with fragment excitation energies as determined from the parameters of postscission components, is estimated to be about 3×10^{-19} s. This gives an estimate of neutrons evaporated during acceleration of the order of 0.02, which is rather small compared to the total number of excess neutrons.

The excess prescission neutrons were used to estimate the dynamical fusion-fission delays. The neutron decay width Γ_n for decay from a compound nucleus at a given excitation energy E_x and spin I is given by [4]

$$\Gamma_n(E_x, I) = \frac{2S_n + 1}{2\pi\rho(E_x, I)} \sum_{I=0}^{\infty} \sum_{J=|I-l|}^{I+l} \int_0^{E_x - B_n} \rho(E_x - B_n - \epsilon_n) T_l(\epsilon_n) d\epsilon_n. \quad (3)$$

From the above expression, we get mean evaporation lifetime given by $\hbar/\Gamma_n$ for the emission of the first neutron at a given excitation energy E_x. The total fusion-fission delay τ_{fission} is obtained by summing the time delays involved in the emission of the observed excess neutrons. The values for τ_{fission} as deduced from this analysis were found to be about $(50 \pm 5) \times 10^{-21}$ and $(35 \pm 5) \times 10^{-21}$ s for the $^{16}O+^{232}Th$ and $^{11}B+^{237}Np$ systems, respectively, for the level density parameters $a_n = A_{CN}/10.0$ and $a_f/a_n = 1.0$. For the $^{12}C+^{232}Th$ and $^{11}B+^{232}Th$ systems, total fusion-fission delays are about $(30 \pm 4) \times 10^{-21}$ and $(17 \pm 3) \times 10^{-21}$ s, respectively, for the same set of parameters. These time scales are in general agreement with the earlier systematics [1,4] for the fusion-fission time scales. It is seen from the above that in the case of the $^{16}O+^{232}Th$ system, there is an extra 40% of the total delay as compared to the $^{11}B+^{237}Np$ system, presumably resulting from the difference in the formation time of the compound nucleus in the two cases. It may be pointed out that this conclusion is not sensitively dependent on the chosen values of a_n and a_f/a_n. The above measured fusion-fission delay can be considered to be made up of three components: transient delay, saddle-to-scission delay, and formation delay. In an earlier study of fission fragment angular distributions, it was suggested that for the $^{16}O+^{232}Th$ system a certain fraction (about 30%) of events lead to preequilibrium fission, which are expected to have smaller formation delay. Considering that the

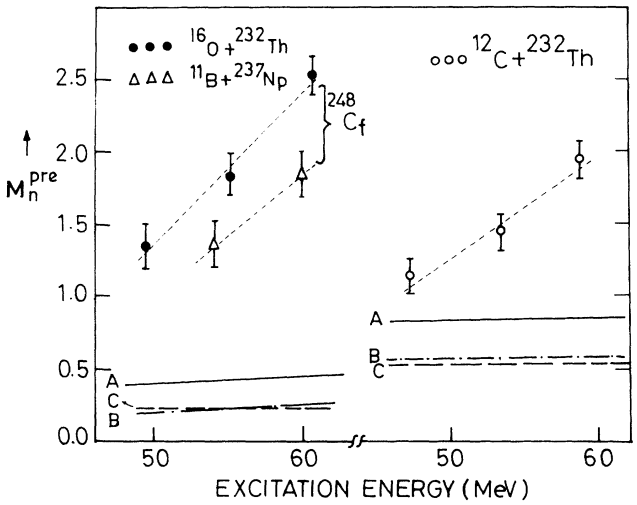

FIG. 6. Comparison of the measured average prescission neutron multiplicity with statistical model calculations. Lines A, B, C correspond to calculations with different sets of level density parameters: (i) $a_n = A/10.0$ MeV^{-1} and $a_f/a_n = 1.0$, (ii) $a_n = A/7.5$ MeV^{-1} and $a_f/a_n = 1.0$, and (iii) $a_n = A/10.0$ MeV^{-1} and $a_f/a_n = 1.02$, respectively.

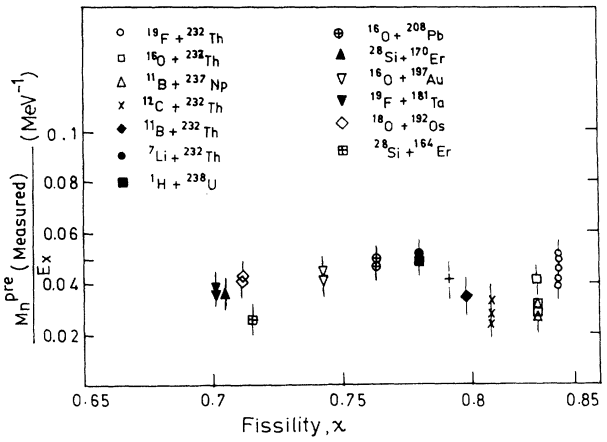

FIG. 7. Systematics of M_n^{pre}/E_x as a function of the compound nucleus fissility.

transient delay and saddle-to-scission delay are expected to be present in both normal and preequilibrium fission events, the effect of inclusion of this component may further increase the difference in the formation times of the normal fusion-fission events for the two systems lying on either side of α_{BG} as deduced above.

IV. SYSTEMATICS OF FUSION-FISSION TIME SCALES

Analyses of several measurements of excess neutrons as a function of mass and excitation energy of the fissioning nucleus have been reported by several groups. We have carried out a global analysis of the relevant experimental data available in the literature [5–9] for compound nuclei with $0.7 < x < 0.84$ using a single set of statistical model parameters. Table I gives the list of systems taken up for the present analysis. It is seen that the data include systems with entrance channel mass asymmetry both below and above the liquid-drop Businaro-Gallone mass asymmetry α_{BG}. The α_{BG} values were calculated using the empirical relation given by Abe [23] as

$$\alpha_{BG} = \begin{cases} 0 & (x < x_{BG}) \\ p\sqrt{\frac{(x-x_{BG})}{(x-x_{BG})+q}} & (x > x_{BG}), \end{cases} \quad (4)$$

with $p = 1.12$, $q = 0.240$, and $x_{BG} = 0.396$.

The full set of data on M_n^{pre} spanning the compound nucleus fissility region of $0.7 < x < 0.84$ and $B_f/T < 4.0$ is shown in Fig. 7, where values of M_n^{pre}/E_x are plotted versus the fissility parameter x. Here B_f is the effective fission barrier averaged over the spin distribution and x is the fissility parameter given by

$$x = \frac{Z^2/A}{50.883\{1 - 1.7826[(N-Z)/A]^2\}}. \quad (5)$$

The data points corresponding to different target-projectile combinations are depicted by different symbols in Fig. 7. In order to determine the number of prescission neutrons $(M_n^{pre})_{stat}$ expected on the basis of the statistical model, calculations were performed with two different codes PACE2 [29] and ALICE [31] with the level density parameter $a_n = A/10$ MeV^{-1} and $a_f/a_n = 1.0$. The results of calculations from these two codes were found to be consistent. The fission barriers entering these calculations were taken from the rotating finite range model of Sierk [32]. The excess number of prescission neutrons, M_n^{pre} (excess), were determined after subtracting the statistical model calculated values of $(M_n^{pre})_{stat}$ from the measured M_n^{pre} and the values of M_n^{pre} (excess) were converted to fission delay $\tau_{fission}$ using the neutron decay width Γ_n, calculated from the statistical model for decay of the compound nucleus at any given excitation energy as discussed in Sec. III. The values of total fission delay $\tau_{fission}$ thus deduced are plotted in Fig. 8 as a function of B_f/T for all systems. As different systems correspond to different fissility and mass asymmetry, the scatter in the overall data in the figure shows that $\tau_{fission}$ also has a

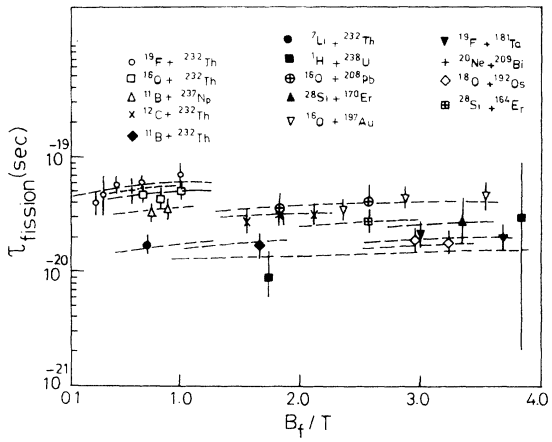

FIG. 8. Total dynamical fusion-fission delay as a function of B_f/T. The dashed lines show fits to the data with Eq. (8).

dependence on fissility and entrance channel mass asymmetry. For a given target-projectile system, however, a systematic dependence of $\tau_{\rm fission}$ on B_f/T can be seen in the figure. As already mentioned earlier, the total fission delay is a sum of three terms:

$$\tau_{\rm fission} = \tau_{\rm tr} + \tau_{\rm ss} + \tau_{\rm fo}. \quad (6)$$

We identify the component $\tau_{\rm tr}$ with the transient delay due to the diffusion from equilibrium configuration to the saddle point. The theoretical framework for calculating the fission probabilities with inclusion of dynamical effects in the fission process has been developed by Weidenmuller and co-workers [11–13] and Grange [14] based on the pioneering work of Kramers [15]. Treating nuclear fission as a diffusion process over the fission barrier, Kramers showed that the fission width is reduced with respect to the Bohr-Wheeler value by a factor (Kramers factor) given by

$$f_k = [(1+\gamma^2)^{1/2} - \gamma], \quad (7)$$

where $\gamma = \beta/2\omega_0$; β is the reduced dissipation coefficient, and ω_0 is the harmonic oscillator frequency cor-

TABLE I. List of systems used in the present analysis.

System	E_x (MeV)	$M_n^{\rm pre}$	x	α	$\alpha_{\rm BG}$	Ref.
	30.5	1.25±0.15				[6]
p+^{238}U			0.78	0.992	0.885	
	120.0	5.80±1.0				[9]
^{7}Li+^{232}Th	105.0	5.50±0.6	0.78	0.941	0.885	[7]
^{11}B+^{232}Th	60.4	2.10±0.15	0.798	0.909	0.886	
	54.1	1.35±0.14				
^{11}B+^{232}Np			0.826	0.911	0.897	
	59.9	1.85±0.16				
	47.4	1.15±0.10				
^{12}C+^{232}Th	53.1	1.45±0.12	0.808	0.902	0.89	Present
	58.8	1.95±0.15				measurements
	49.5	1.35±0.16				
^{16}O+^{232}Th	55.2	1.82±0.15	0.826	0.871	0.897	
	60.8	2.53±0.18				
	54.6	2.00±0.16				
	64.8	2.70±0.23				
^{19}F+^{232}Th	73.1	3.32±0.29	0.834	0.849	0.90	[5]
	81.4	4.07±0.50				
	86.0	4.39±0.40				
	59.4	2.80±0.30				
^{16}O+^{208}Pb			0.763	0.857	0.871	[8]
	72.5	3.40±0.50				
	63.0	2.67±0.23				
^{16}O+^{197}Au	72.2	3.28±0.20	0.743	0.85	0.861	[5]
	80.5	3.35±0.34				
^{28}Si+^{170}Er	84.1	3.00±0.37	0.704	0.717	0.84	[5]
^{28}Si+^{164}Er	78.4	2.00±0.25	0.715	0.708	0.846	[5]
	88.6	3.22±0.30				
^{19}F+^{181}Ta			0.701	0.81	0.838	[5]
	97.6	3.72±0.36				
	88.1	3.65±0.34				
^{18}O+^{192}Os			0.711	0.829	0.844	[5]
	91.8	3.86±0.37				
^{20}Ne+^{209}Bi	76.0	3.20±0.40	0.792	0.825	0.884	[7]

responding to the saddle point. It is seen [11–14] that the diffusion from the equilibrium configuration to the saddle point takes place over a finite transient time τ_{tr}, which can be defined as the time during which the fission width rises to 90% of its final quasistationary limit. Thus the disintegration constant λ_f for fission becomes a time-dependent quantity eventually reaching the asymptotic value λ_f^{∞}. For mathematical simplicity, λ_f is assumed to have the same form as that for the charging of a capacitor

$$\lambda_f(t) = \lambda_f^{\infty}[1 - \exp(-t/\tau_{tr})], \tag{8}$$

where

$$\lambda_f^{\infty} = \frac{\Gamma_f^{BW}}{\hbar}[(1+\gamma^2)^{1/2} - \gamma],$$

where Γ_f^{BW} is the Bohr-Wheeler value.

For overdamped motion ($\gamma > 1$), the transient delay τ_{tr} can be expressed as

$$\tau_{tr} = \frac{\beta}{2\omega_1^2} \ln(10B_f/T), \tag{9}$$

where β is the reduced dissipation coefficient and ω_1 is the curvature of the potential energy corresponding to the ground state minimum of the fissioning nucleus.

On the basis of qualitative arguments, β is expected to be a smooth function of temperature T, with β approaching zero as T tends to zero. Such a behavior was inferred [33] from the study of the effect of friction on spontaneous fission half-lives, and an upper limit to β of 3×10^{20} s^{-1} was obtained. It is further reasonable to assume that τ_{SS} depends mainly on fissility x and is not very sensitive to the temperature of the fissioning nucleus. It is expected that the value of τ_{fo} will depend on the entrance channel mass asymmetry α, and one may reasonably assume it to be independent of bombarding energy in a limited region. We can, therefore, parametrize the above fusion-fission delay $\tau_{fission}$ with the expression

$$\tau_{fission} = aT \ln(10B_f/T) + k(x,\alpha), \tag{10}$$

assuming β to be proportional to T. The first term corresponds to the transient delay, and the second term $k(x,\alpha)$ corresponds to the sum of the formation time and saddle-to-scission transition time.

The experimental data on $\tau_{fission}$ were fitted to Eq. (10) to deduce the values of a and k. The fits to the data are shown by the dashed lines in Fig. 8. From these smooth fits, it is now possible to deduce values of $\tau_{fission}$ for various systems at a fixed value of B_f/T. The deduced values of $\tau_{fission}$ corresponding to a typical case of $B_f/T = 1.0$ for the various systems have been plotted against the fissility parameter x in Fig. 9(a). It is seen from the figure that the fission delay, in general, increases with x, which is expected due to the increase in τ_{SS} with fissility [16,17]. It is interesting to note that the data points are seen to bunch broadly into two groups corresponding to composite systems with entrance channel mass asymmetry $\alpha < \alpha_{BG}$ and $\alpha > \alpha_{BG}$. It is clear that this bunching of the data into two groups arises due to the behavior of $k(x,\alpha)$ with respect to the mass asymmetry α. In order to see this more explicitly, we have deduced the values of $\tau_{fission}$ from the fits of Fig. 8 corresponding to $B_f/T = 0.1$. In this case, the first term in Eq. (10) vanishes and $\tau_{fission}$ then corresponds to $k(x,\alpha)$ alone, which is the sum of τ_{SS} and τ_{fo}. Figure 9(b) shows the values of $(\tau_{SS} + \tau_{fo})$ thus deduced as a function of x. As expected, the data are clearly seen to be bunched into two separate groups corresponding to $\alpha < \alpha_{BG}$ and $\alpha > \alpha_{BG}$, and for each case $\tau_{SS} + \tau_{fo}$ increases with x. The dashed lines in Figs. 9(a) and 9(b) show the fits to the data points for the two groups. This figure also brings out two important features. For systems with $\alpha > \alpha_{BG}$ where the formation time of the compound nucleus, τ_{fo}, is expected to be small, it may be reasonable to assign the deduced delay entirely to τ_{SS}, which is found to vary from 5×10^{-21} to 30×10^{-21} s in the present fissility range. Based on the same reasoning, the difference in the delay for the two groups can be ascribed to τ_{fo} for systems with $\alpha < \alpha_{BG}$, which is found to be about $(10\text{–}15) \times 10^{-21}$ s. The difference in the delays plotted in Figs. 9(a) and 9(b) corresponds to the value of transient delay τ_{tr} [on the basis of Eq. (9)], and the values of τ_{tr}, thus deduced for $B_f/T = 1.0$, are shown in Fig. 9(c). In this way we are able to deduce the values of τ_{tr} alone for

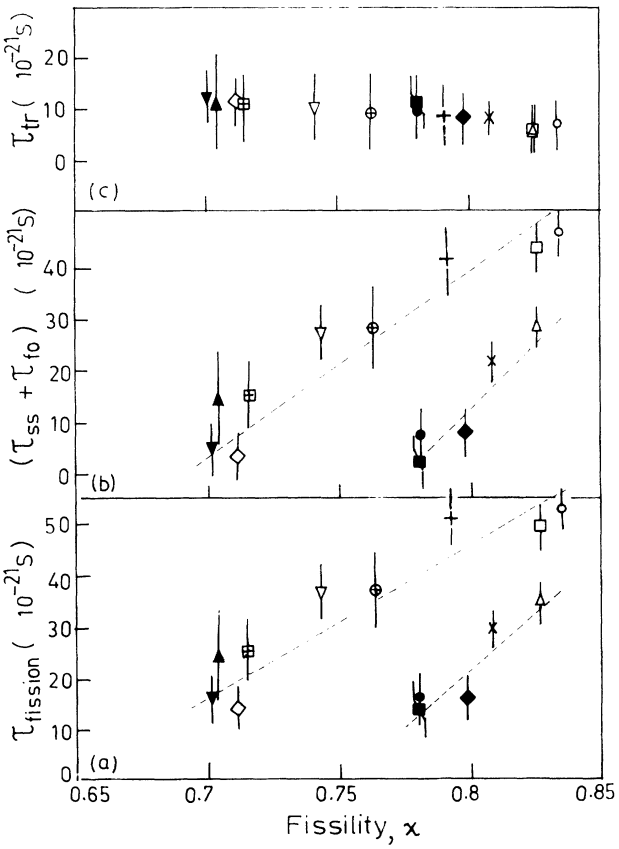

FIG. 9. (a) Total dynamical fusion-fission delay, deduced for $B_f/T = 1.0$, against the fissility parameter x. (b) Sum of saddle-to-scission delay τ_{SS} and formation delay τ_{fo} as a function of x. (c) Transient delay τ_{tr} at $B_f/T = 1.0$ versus fissility parameter x.

various target-projectile systems. It is seen that τ_{tr} lies in the range of $(5\text{–}10)\times10^{-21}$ s for the various systems. This range of values is in good agreement with theoretical predictions of Bhatt, Grange, and Hiller [34] for the ^{248}Cf system.

We have also analyzed the data in Fig. 8 assuming β to be independent of temperature and did not find any significant change in the quality of fits from that shown in Fig. 8. It is found that reasonably good fits for the entire set of data are obtained with $\beta = 7 \times 10^{21}$ s^{-1}, assuming a value of $\omega_1 = 1 \times 10^{-21}$ s. The transient delay, deduced for $B_f/T = 1.0$, is found to be 8.1×10^{-21} s for all systems, and the features seen in the fusion-fission delay as a function of fissility and mass asymmetry remain unchanged but for small differences in the absolute values of the individual components of delays.

The absolute values of the time scales derived above are sensitive to the level density parameter a_n. In the present work, the value of a_n has been taken to be $A/10.0$ MeV^{-1}, but the relative intercomparison with fissility and mass asymmetry is not found to be sensitive to the above choice.

V. SUMMARY AND CONCLUSIONS

To summarize, in the present work, we have experimentally investigated entrance channel effects in the prescission neutron multiplicities in fusion-fission reactions by studying the target-projectile systems lying on either side of the Businaro-Gallone point. The measured prescission neutron multiplicites are found to be higher for the ^{16}O+^{232}Th system as compared to the ^{11}B+^{237}Np, ^{11}B+^{232}Th, and ^{12}C+^{232}Th systems, implying for the former case a larger fusion-fission delay resulting from larger dynamical time during formation of the compound nucleus. We have carried out a systematic analysis of the available prescission neutron multiplicity data in the compound nuclear fissility range of $0.7 < x < 0.84$ to deduce the individual dynamical delays, namely, the transient time, saddle-to-scission transition time, and compound nuclear formation time, which are involved in the different stages of the fusion-fission dynamics. The present studies have brought out the dependence of fusion-fission delays on the values of B_f/T and fissility of the compound nucleus produced in heavy-ion reactions.

ACKNOWLEDGMENTS

We are thankful to Dr. V. S. Ramamurthy for many useful discussions on this work. We thank Dr. R. P. Anand, M. S. Samant, L. M. Pant, and B. K. Nayak for their valuable help during the course of this experiment, and also the operating staff of Pelletron accelerator for making available the required beams.

[1] J. O. Newton, Pramana **39**, 175 (1989).
[2] S. S. Kapoor, in Proceedings of Consultants Meeting on Physics of Neutron Emission in Fission, Mito City, Japan [International Nuclear Data Committee (NDS) **220**, 221 (1989)].
[3] D. J. Hilscher, H. Rossner, B. Cramer, B. Gebauer, U. Jahnke, M. Lehmann, E. Schwinn, M. Wilpert, T. Wilpert, H. Frobeen, E. Mordhorst, and W. Scobel, Phys. Rev. Lett. **62**, 1099 (1989).
[4] D. J. Hinde, D. Hilscher, H. Rossner, B. Gebauer, M. Lehmann, and M. Wilepert, Phys. Rev. C **45**, 1229 (1992).
[5] J. O. Newton, D. J. Hinde, R. J. Charity, J. R. Leigh, J. J. M. Bokhorst, A. Chatterjee, G. S. Foote, and S. Ogaza, Nucl. Phys. **A483**, 126 (1988).
[6] M. Strecker, R. Wein, P. Plischke, and W. Scobel, Phys. Rev. C **41**, 2172 (1990).
[7] D. J. Hinde, H. Ogata, M. Tanaka, T. Shimoda, N. Takahashi, A. Shinohara, S. Wakamatsu, K. Katori, and H. Okamura, Phys. Rev. C **39**, 2268 (1989).
[8] H. Rossner, D. J. Hinde, J. R. Leigh, J. P. Lestone, J. O. Newton, J. X. Wei, and S. Elfstrom, Phys. Rev. C **45**, 719 (1992).
[9] E. Cheifetz, Z. Fraenkel, J. Galin, M. Lefort, J. Peter, and X. Tarrago, Phys. Rev. C **2**, 256 (1970).
[10] A. Gavron, A. Gayer, J. Boissevin, H. C. Britt, J. R. Nix, A. J. Sierk, P. Grange, S. Hassani, H. A. Weidenmuller, J. R. Beene, F. Plasil, G. R. Young, G. A. Petitt, and C. Butler, Phys. Lett. B **176**, 312 (1986).
[11] H. A. Weidenmuller, Nucl. Phys. **A471**, 1c (1987).
[12] H. A. Weidenmuller and Zhang Jing Shang, Phys. Rev. C **29**, 879 (1984).
[13] P. Grange, J-Q. Li, and H. A. Weidenmuller, Phys. Rev. C **27**, 2063 (1983).
[14] P. Grange, Nucl. Phys. **A428**, 37c (1984).
[15] H. A. Kramers, Physica **7**, 284 (1940).
[16] H. Hoffmann and J. R. Nix, Phys. Lett. **122B**, 117 (1983).
[17] J. R. Nix, A. J. Sierk, H. Hoffman, F. Scheuter, and D. Vautherin, Nucl. Phys. **A429**, 239 (1984).
[18] W. U. Schroder and J. R. Huizenga, in *Treatise in Heavy-Ion Science*, edited by D. A. Bromley (Plenum, New York, 1984), Vol. 2, p. 115.
[19] V. S. Ramamurthy and S. S. Kapoor, Phys. Rev. Lett. **54**, 178 (1985).
[20] V. S. Ramamurthy, S. S. Kapoor, R. K. Choudhury, A. Saxena, D. M. Nadkarni, A. K. Mohanty, B. K. Nayak, S. V. S. Ssastry, S. Kailas, A. Chatterjee, P. Singh, and A. Navin, Phys. Rev. Lett. **65**, 25 (1990).
[21] U. L. Businaro and S. Gallone, Nuovo Cimento **5**, 315 (1957).
[22] K. T. R. Davies and A. J. Sierk, Phys. Rev. C **31**, 915 (1985).
[23] M. Abe, KEK Report No. 86-26, KEK TH-28, 1986.
[24] D. G. Madland and J. R. Nix, in *Proceedings of the Conference on Nuclear Data for Science and Technology*, Antwerp, Belgium, 1982, edited by K. H. Bockhoff (Reidel, Dordrecht, 1983), p. 473.

[25] E. Holub, D. Hilscher, G. Ingold, U. Jahnke, H. Orf, and H. Rossner, Phys. Rev. C **28**, 252 (1983).
[26] V. E. Viola, Jr., K. Kwiatowski, and M. Walker, Phys. Rev. C **31**, 1550 (1985).
[27] K. L. Le Conteur and D. W. Lang, Nucl. Phys. **13**, 32 (1959).
[28] D. W. Lang, Nucl. Phys. **53**, 113 (1964).
[29] A. Gavron, Phys. Rev. C **21**, 230 (1980).
[30] V. P. Eismont, Sov. J. At. Energy **19**, 1000 (1965).
[31] M. Blann, LLNL Report No. UCID-20169, 1984 (unpublished).
[32] A. J. Sierk, Phys. Rev. C **33**, 2039 (1986).
[33] N. R. Davidviren and H. A. Weidenmuller, Phys. Lett. B **186**, 267 (1987).
[34] K. H. Bhatt, P. Grange, and B. Hiller, Phys. Rev. C **33**, 954 (1986).